Measurement of the Forward-Backward Asymmetry of $t\bar{t}$ in the Two Lepton Final State at CDF

Ziqing Hong[1]
[1] *Texas A&M University*
(Dated: July 14, 2014)

The forward-backward asymmetries of the top-quark pairs produced in proton-antiproton collisions and the charged leptons from the cascade decay of top-quark pairs serve as a test of the standard model (SM) as well as a probe for the physics beyond the SM. We work with the full dataset collected with the Collider Detector at Fermilab during Tevatron run II in the final states that contain two charged leptons, with an integrated luminosity of 9.1 fb^{-1}, to produce a full analysis of the asymmetries of the top-quark pairs and their decay products. We have measured the inclusive forward-backward asymmetry of the charged lepton pseudorapidities from top-quark-pair events. The leptonic forward-backward asymmetry, $A^l_{\rm FB}$, is measured to be 0.072 ± 0.060 and the leptonic pair forward-backward asymmetry, $A^{ll}_{\rm FB}$, is measured to be 0.076 ± 0.082, compared with the next-to-leading order standard model predictions of $A^l_{\rm FB} = 0.038 \pm 0.003$ and $A^{ll}_{\rm FB} = 0.048 \pm 0.004$, respectively. Additionally, we present the combined measurement of $A^l_{\rm FB}$ with the previous result in the final state involving a single lepton and hadronic jets; the combined asymmetry $A^l_{\rm FB} = 0.090^{+0.028}_{-0.026}$ is the most precise measurement to date. We also show the prospect of measuring the inclusive forward-backward asymmetry of the top-quark pairs ($A^{t\bar{t}}_{\rm FB}$) in the final states with two charged leptons, as well as the possibility of producing the combined results of $A^{t\bar{t}}_{\rm FB}$, $A^l_{\rm FB}$ and $A^{ll}_{\rm FB}$ at Tevatron.

1. INTRODUCTION

The Fermi National Accelerator Laboratory's Tevatron Run II collided protons against antiprotons at $\sqrt{s} = 1.96$ TeV from 2003 to 2011. Top and anti-top quark pairs ($t\bar{t}$) can be produced via quark-antiquark annihilation (85%) and gluon-gluon fusion (15%). The forward-backward asymmetry $A_{\rm FB}$ of the $t\bar{t}$ system ($A^{t\bar{t}}_{\rm FB}$) is an interesting observable providing a chance to test the Standard Model (SM) and to probe physics beyond the SM.

Recent measurements of the $A^{t\bar{t}}_{\rm FB}$ at the Fermilab Tevatron [1–3] have shown anomalously large values compared to the predictions from SM at next-to-leading order (NLO) [4]. This could be a hint for the physics beyond the SM. To look for new evidence for or against this hint for new physics, we can measure a separate set of observables are the forward-backward asymmetry of the charged lepton pseudorapidities that can originate from the cascade decays of the top quarks, the so-called leptonic forward-backward asymmetry ($A^l_{\rm FB}$), and the leptonic pair forward-backward asymmetry ($A^{ll}_{\rm FB}$) for the final state with two charged leptons (dilepton final state) [5].

In the forthcoming sections, a summary of the theoretical motivations for the measurement of $A^{t\bar{t}}_{\rm FB}$, $A^l_{\rm FB}$ and $A^{ll}_{\rm FB}$ will be presented. A description of the CDF detector, the event selection criteria used to select a sample enriched by the $t\bar{t}$ events in the dilepton final state and the estimation of background processes follow that. We then describe a study of the methodology to measure the $A^l_{\rm FB}$ and $A^{ll}_{\rm FB}$, and show the results obtained with CDF data. A combined result of $A^l_{\rm FB}$ at CDF with both the lepton+jets and the dilepton final state is also presented. All the analysis will use the full dataset collected by the CDF detector through Run II of the Fermilab Tevatron, corresponding to an integrated luminosity of 9.1 fb^{-1}. We conclude with the prospect of measuring $A^{t\bar{t}}_{\rm FB}$ in the dilepton final state and the Tevatron combination of $A^{t\bar{t}}_{\rm FB}$, $A^l_{\rm FB}$ and $A^{ll}_{\rm FB}$.

2. MOTIVATION

The forward-backward asymmetry of the $t\bar{t}$ system produced at the Fermilab Tevatron can be defined as

$$A^{t\bar{t}}_{\rm FB} = \frac{N(\Delta y > 0) - N(\Delta y < 0)}{N(\Delta y > 0) + N(\Delta y < 0)}, \qquad (1)$$

where N is the number of events, y is the rapidity of the (anti-)top quark, and $\Delta y = y_t - y_{\bar{t}}$. Previous measurements of $A^{t\bar{t}}_{\rm FB}$ at CDF with 9.4 fb^{-1} and at D0 with 5.4 fb^{-1} data in the final state with only one charged lepton and hadronic jets (lepton+jets final state) have indicated a larger $A^{t\bar{t}}_{\rm FB}$ [1, 2] than would be expected from the standard model. Similar measurement has been done at CDF in the dilepton final state with 5.1 fb^{-1} data [6] which also shows larger $A^{t\bar{t}}_{\rm FB}$ value than expected. The asymmetry in the differential cross section of the $t\bar{t}$ system has also been probed in other ways. For example, the angular distribution of cross section of $t\bar{t}$ system has been studied in the lepton+jets final state at CDF [3], observing an excess in the coefficient of the linear dependent term of $\cos\theta_t$ in the $t\bar{t}$ differential cross section,

where $\cos\theta_t$ is the angle between the top-quark momentum and the incoming proton momentum as measured in the $t\bar{t}$ center-of-mass frame. This is of great interest, as new particles or interactions could cause the $A_{\rm FB}^{t\bar{t}}$ to be different from SM-only predictions [7].

As the anomalously large $A_{\rm FB}^{t\bar{t}}$ is suggestive for physics beyond the SM, we can look for more evidence for or against new physics with a separate set of observables, $A_{\rm FB}^{l}$ and $A_{\rm FB}^{ll}$. We can define the $A_{\rm FB}^{l}$ as

$$A_{\rm FB}^{l} = \frac{N(q_l\eta_l > 0) - N(q_l\eta_l < 0)}{N(q_l\eta_l > 0) + N(q_l\eta_l < 0)} \quad (2)$$

where N is the number of leptons, q is the lepton charge, and η is the pseudorapidity of the lepton. Similarly, since there are two leptons detected in each event in the dilepton final state, the $A_{\rm FB}^{ll}$ can be defined as

$$A_{\rm FB}^{ll} = \frac{N(\Delta\eta > 0) - N(\Delta\eta < 0)}{N(\Delta\eta > 0) + N(\Delta\eta < 0)} \quad (3)$$

where $\Delta\eta = \eta_{l^+} - \eta_{l^-}$.

This set of observables are of equal importance, since the forward-backward asymmetry of the charged leptons can originate from the asymmetry in the production direction of their parent top quarks. In addition, the $A_{\rm FB}^{l}$ and $A_{\rm FB}^{ll}$ can deviate further from their SM predictions in the scenarios that the top quarks are produced with a certain polarization. For example, the resonant production of $t\bar{t}$ pairs via a hypothetical gluon with axial couplings ("axigluons") could cause the $A_{\rm FB}^{t\bar{t}}$ to deviate from its SM value; various axigluon couplings to the top quarks could produce the same value of $A_{\rm FB}^{t\bar{t}}$, but with very different values of $A_{\rm FB}^{l}$ and $A_{\rm FB}^{ll}$ [8].

There are also advantages in measuring the $A_{\rm FB}^{l}$ and $A_{\rm FB}^{ll}$ over the measurement of the $A_{\rm FB}^{t\bar{t}}$ itself. The ability to reconstruct the 4-momentums of both the top and anti-top quarks is limited, and can have large systematic uncertainties. The reconstruction of the $t\bar{t}$ system is especially difficult in dilepton final state, due to the ambiguity of b-jet and $\bar{b}$-jet and the distribution of the $\not\!\!E_T$ between the two neutrinos. On the other hand, the measurement of the $A_{\rm FB}^{l}$ and $A_{\rm FB}^{ll}$ mainly relies on the directions of the charged lepton paths in the detector, which are measured with high precision. Thus, the measurement of the $A_{\rm FB}^{l}$ and $A_{\rm FB}^{ll}$ can be done with better precision, and could yield information about both the inherit forward-backward asymmetry of the $t\bar{t}$ system as well as its polarization.

Since many models of new physics predict very different values of $A_{\rm FB}^{l}$, we simulate $t\bar{t}$ production and decay in various scenarios to study the range of different hypothetical $A_{\rm FB}^{l}$ and $A_{\rm FB}^{ll}$ values. The POWHEG $t\bar{t}$ MC sample serves as best estimate of the SM. It gives values of $A_{\rm FB}^{l} = 0.024$ and $A_{\rm FB}^{ll} = 0.030$. These predictions are different from the NLO SM calculation in [4] since the simulation does not contain the electroweak corrections [9]. Two samples generated with PYTHIA [10] and ALPGEN [11] serve as the samples simulating the SM at the leading order (LO). Three $t\bar{t}$ MC samples with a class of relatively light and wide axigluons (with masses at 200 GeV/c^2 and widths at 50 GeV) with left-handed, right-handed, and axial axigluon couplings to the quarks [8] serve as benchmark simulation samples to model various SM extensions. Each predicts an $A_{\rm FB}^{t\bar{t}}$ value that is similar to the measured value by the CDF Collaboration [1], but the polarization of the top quarks produces different values of $A_{\rm FB}^{l}$ and $A_{\rm FB}^{ll}$. Table I shows the values of $A_{\rm FB}^{l}$ and $A_{\rm FB}^{ll}$ at parton level for each MC sample we used, together with the NLO theoretical calculation with QCD and EWK correction from Ref. [4].

Model	$A_{\rm FB}^{l}$ (Generator Level)	$A_{\rm FB}^{ll}$ (Generator Level)	Description
AxiL	-0.063(2)	-0.092(3)	Tree-level left-handed axigluon (m = 200 GeV/c^2, Γ = 50 GeV/c^2)
AxiR	0.151(2)	0.218(3)	Tree-level right-handed axigluon (m = 200 GeV/c^2, Γ = 50 GeV/c^2)
Axi0	0.050(2)	0.066(3)	Tree-level unpolarized axigluon (m = 200 GeV/c^2, Γ = 50 GeV/c^2)
ALPGEN	0.003(1)	0.003(2)	Tree-level Standard Model
PYTHIA	0.000(1)	0.001(1)	LO Standard Model
POWHEG	0.024(1)	0.030(1)	NLO Standard Model
Theory	0.038(3)	0.048(4)	NLO SM calculation [4]

TABLE I: The MC samples used to study the $t\bar{t}$ system in this analysis, together with the parton level $A_{\rm FB}^{l}$ and $A_{\rm FB}^{ll}$ predicted by the corresponding physics model, as well as NLO SM calculation. The uncertainties listed with the MC samples are statistical only.

The measurement of the $A_{\rm FB}^{l}$ of the $t\bar{t}$ system has been performed in the lepton+jets final state at CDF with the full dataset [12], in which case a $\sim 2\sigma$ deviation from NLO SM prediction is observed. There are similar measurements from D0 with both lepton+jets and dilepton final states [13, 14], which show results that are consistent with the NLO SM prediction.

3. CDF DETECTOR, EVENT SELECTION AND BACKGROUND ESTIMATION

In this analysis, we use the full dataset collected by the CDF detector during Run II of the Tevatron corresponding to an integrated luminosity of 9.1 fb^{-1}.

The Tevatron, located at the Fermi National Laboratory, is a $p\bar{p}$ collider with center-of-mass energy of 1.96 TeV. The Tevatron has two multi-purpose detectors, the Collider Detection at Fermilab (CDF, the one we use in this analysis) and D0. The CDF detector, described in detail elsewhere [15], is a general-purpose particle detector employing a large charged-particle tracking volume inside a solenoidal magnetic field coaxial with the beam direction, surrounded by calorimeters and muon detectors. We use a cylindrical coordinate system with the origin at the center of the CDF detector, z pointing in the direction of the proton beam, θ and ϕ representing the polar and azimuthal angles, respectively, and pseudorapidity defined by $\eta = -\ln\tan(\theta/2)$. The transverse momentum p_T (transverse energy E_T) is defined to be $p\sin\theta$ ($E\sin\theta$).

We follow the event selection criteria that was used in measuring the top pair cross section in the dilepton final state [16], with the dilepton invariant mass (m_{ll}) requirement raised to 10 GeV/c^2 to prevent potential mismodelling in low dilepton invariant mass region. The event selection criteria is summarized in Table II.

Baseline Cuts	Exactly two leptons with $E_T > 20$ GeV and passing standard identification requirements with following modifications -COT radius exit > 140 cm for CMIO -$\chi^2/ndf < 2.3$ for muon tracks At least one trigger lepton At least one tight and isolated lepton At most one lepton can be loose and/or non-isolated
	$\not\!\!E_T > 25$ GeV, but $\not\!\!E_T > 50$ GeV when there is any lepton or jet within 20° of the direction of $\not\!\!E_T$
	MetSig ($= \frac{\not\!\!E_T}{\sqrt{E_T^{sum}}}$) > 4 $\sqrt{\text{GeV}}$ for ee and $\mu\mu$ events where 76 GeV/c^2 < m_{ll} < *106* GeV/c^2
	Dilepton invariant mass > 10 GeV/c^2
Signal Cuts	Two or more jets with $E_T > 15$ GeV within $\|\eta\| < 2.5$
	$H_T > 200$ GeV
	Opposite sign of two leptons

TABLE II: The top dilepton event selection criteria.

Several physical processes can mimic the signature of top pairs with dilepton final state, such as Z/γ^*+jets production, W+jets production, diboson production (WW, WZ, ZZ and $W\gamma$), and situations where one of the W bosons from $t\bar{t}$ decays hadronically and one of the b-quark jet or jet from hadronic W decay is misidentified as a charged lepton. We follow a similar prescription as used in the top pair cross section measurement in the dilepton final state for background modelling. The prescription is constituted of a mixture of Monte Carlo simulations and data-based techniques. A collection of MC samples are generated for this purpose. WW, WZ and ZZ processes are simulated with PYTHIA MC generator [10], $W\gamma$ process is simulated with BAUR MC generator [17], and Z/γ^*+jets processes are simulated with ALPGEN MC generator [11]. PYTHIA is used for modelling parton hadronization and underlying events for all MC simulations. A GEANT-based simulation, CDFSIM [18, 19], is used to model the CDF detector. The estimation of contamination from the diboson processes are obtained by normalizing the corresponding MC samples to the integrated luminosity collected in data with their predicted production cross section. The contamination from the W+jets process is estimated with a data-based technique where the probability of a jet faking a charged lepton is derived from a separate dataset [16].

The contamination from Z/γ^*+jets where Z/γ^* decays to two electrons or two muons are done with a data-MC hybrid method. The MC samples are normalized to data after subtracting off components other than $Z/\gamma^* \to$ ee/$\mu\mu$ according to the number of events within the window of 76 GeV/c^2 < m_{ll} < 106 GeV/c^2 after requiring high $\not\!\!E_T$. As an improvement from the cross section measurement [16], we use a more sophisticated method to estimate the contamination from the $Z/\gamma^* \to \tau\tau$ process and the $Z/\gamma^* \to ee/\mu\mu$ process which are misidentified as eμ final state by applying two scale factors derived with $Z/\gamma^* \to ee/\mu\mu$ process within the window of 76 GeV/c^2 < m_{ll} < 106 GeV/c^2 to correct for the mismodeling of the total event rate and $\not\!\!E_T$ distribution in the MC simulations.

CDF Run II Preliminary (9.1 fb^{-1})

$t\bar{t}$ Dilepton Signal Events per Dilepton Flavor Category				
Source	ee	$\mu\mu$	eμ	$\ell\ell$
WW	5.5±1.1	4.2±0.8	11.4±2.3	21.1±4.2
WZ	2.7±0.5	1.6±0.3	1.6±0.3	5.8±1.0
ZZ	1.7±0.3	1.3±0.2	0.7±0.1	3.7±0.5
$W\gamma$	0.7±0.8	-	-	0.7±0.8
$Z/\gamma^* \to \tau\tau$	4.4±0.8	3.4±0.6	9.3±1.6	17.0±2.8
$Z/\gamma^* \to ee + \mu\mu$	19.8±2.1	10.4±1.8	3.3±1.5	33.5±3.9
W+jets Fakes	12.4±3.8	14.6±4.7	36.8±11.3	63.8±17.0
$t\bar{t}$ Non-Dilepton	3.3±0.2	3.3±0.2	8.0±0.4	14.6±0.8
Total background	50.5±5.8	38.8±5.6	71.0±12.7	160.3±21.2
$t\bar{t}$ ($\sigma = 7.4$ pb)	96.0±4.6	90.8±4.4	221.4±10.6	408.2±19.4
Total SM expectation	146.4±10.2	129.6±9.7	292.4±23.1	568.5±40.3
Observed	147	139	283	569

TABLE III: Table of expected number of events in data corresponds to 9.1fb^{-1} with the observed number of events passing all event selections, listed by lepton flavors.

There are $t\bar{t}$ events where one of the W boson from the top pair decays hadronically, and one jet (either a b-quark jet or a jet from the hadronic W decay) is misidentified as a charged lepton constituting a significant portion of the events in our sample. Since at least one of the leptons identified in such events is not from W leptonic decay, the pseudorapidities of the charged leptons don't follow the same distribution as the signal. We estimate this contribution with POWHEG $t\bar{t}$ MC sample after normalizing sample with the best theoretical prediction of the $t\bar{t}$ production cross section of 7.4 pb, and put these events into a background category, named "$t\bar{t}$ non-dilepton".

Table III shows the expected number of events from the background processes and the $t\bar{t}$ signal estimated with POWHEG $t\bar{t}$ MC sample, together with the observed number of events in the signal region, listed by lepton flavors. The agreement is excellent.

4. $A_{\rm FB}^l$ AND $A_{\rm FB}^{ll}$ MEASUREMENT METHODOLOGY

Due to the limited detector coverage ($|\eta| < 2$ for electrons and $|\eta| < 1.1$ for muons), the imperfect detector acceptance, the smearing due to detector response and contamination from non-$t\bar{t}$ sources, a correction and extrapolation procedure is needed to measure the inclusive parton level $A_{\rm FB}^l$ and $A_{\rm FB}^{ll}$ from data. To do so, we follow the same procedure used in measuring the $A_{\rm FB}^l$ in the lepton+jets final state [14]. In this section of the proposal, we describe the methodology, and show a study of this

methodology and the validation of this methodology in the dilepton final state. Note that while we will be using the same methodology for measuring the $A^l_{\rm FB}$ as well as the $A^{ll}_{\rm FB}$, our description here will only mention $A^l_{\rm FB}$ explicitly.

4.1. Methodology Overview

Figure 1 shows the $q_l\eta_l$ distribution at parton level for the $t\bar{t}$ MC samples described in Table I. We note that they span the range of possible values of $A^l_{\rm FB}$ from -6% to 15%. Next we outline the key steps of this methodology, following the prescription in Ref. [12, 20].

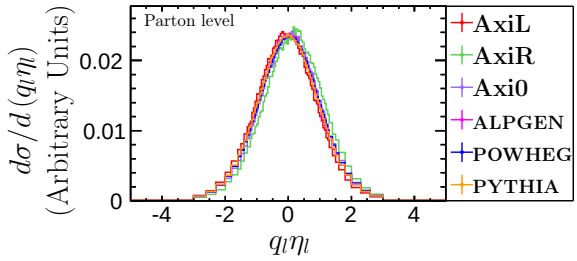

FIG. 1: The $q_l\eta_l$ distribution for leptons from MC samples with various physics models.

As described in Ref. [12, 20], the $q_l\eta_l$ distribution of the leptons can be decomposed into a symmetric part of the distribution (the $\mathcal{S}(q_l\eta_l)$ term) and an asymmetric part of the distribution (the differential $A_{\rm FB}$, or the $\mathcal{A}(q_l\eta_l)$ term) using the following formulas in the range $q_l\eta_l \geq 0$:

$$\mathcal{S}(q_l\eta_l) = \frac{\mathcal{N}(q_l\eta_l) + \mathcal{N}(-q_l\eta_l)}{2}, \text{ and} \tag{4a}$$

$$\mathcal{A}(q_l\eta_l) = \frac{\mathcal{N}(q_l\eta_l) - \mathcal{N}(-q_l\eta_l)}{\mathcal{N}(q_l\eta_l) + \mathcal{N}(-q_l\eta_l)}, \tag{4b}$$

where $\mathcal{N}(q_l\eta_l)$ represents the number of events as a function of $q_l\eta_l$. With this, the $A^l_{\rm FB}$ defined in Eqn. 2 can be rewritten in terms of $\mathcal{S}(q_l\eta_l)$ and $\mathcal{A}(q_l\eta_l)$ as:

$$A^l_{\rm FB} = \frac{\int_0^\infty {\rm d}x\ [\mathcal{A}(x)\cdot\mathcal{S}(x)]}{\int_0^\infty {\rm d}x'\ \mathcal{S}(x')}. \tag{5}$$

The $\mathcal{S}(q_l\eta_l)$ term and the $\mathcal{A}(q_l\eta_l)$ term distributions from the benchmark samples are shown in Fig. 2a and Fig. 2b, respectively. We can readily see that the variation of the $\mathcal{S}(q_l\eta_l)$ term among the benchmark $t\bar{t}$ samples is small, so choosing any one of them for the measurement introduces an uncertainty that is tiny compared to the dominant uncertainties. We will come back to the small differences for $q_l\eta_l < 0.2$ and show why they do not have much affect on the measurement. On the other hand, the $\mathcal{A}(q_l\eta_l)$ term varies significantly from model to model. The $\mathcal{A}(q_l\eta_l)$ term has been well described in the region $|q_l\eta_l| < 2.0$ using the empirically determined functional form of

$$\mathcal{A}(q_l\eta_l) = a\cdot\tanh\left(\frac{1}{2}q_l\eta_l\right) \tag{6}$$

where a is a free parameter that is directly related to the final asymmetry. Best fits of the data to the $a\cdot$tanh model from Eqn. 6 are also shown in Fig. 2b. While the $\mathcal{A}(q_l\eta_l)$ term is well modeled in the region where $q_l\eta_l < 2.5$, it is not as good above 2.5. The comparison between the predicted $A^l_{\rm FB}$ and the $A^l_{\rm FB}$ obtained with a measured value of a in Eqn. 6 from the $\mathcal{A}(q_l\eta_l)$ term (restricting the fit within the region $q_l\eta_l < 2.0$ to simulate the detector) is shown in Fig. 3. The differences are on the order of a fraction of a percent, which is tiny compared to the dominant uncertainties in measurements [12, 20].

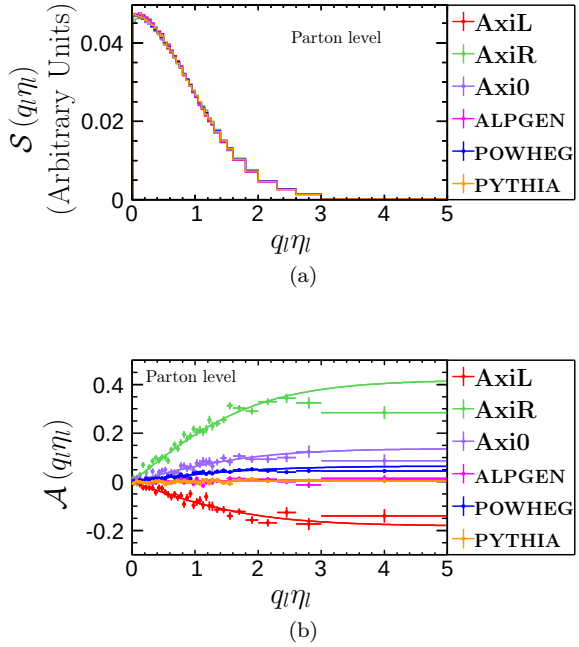

FIG. 2: The $\mathcal{S}(q_l\eta_l)$ term (a) and the $\mathcal{A}(q_l\eta_l)$ term (b) of the $q_l\eta_l$ distribution from various physics models. The lines in (b) correspond to the best fits from the $a\cdot\tanh$ model.

The strategy of this method is to measure the free parameter a from data, and use the symmetric part of parton level $q_l\eta_l$ distribution from $t\bar{t}$ simulation sample to get the parton level $A^l_{\rm FB}$. Note that since only the asymmetric part of detector response contributes to the asymmetric part of $q_l\eta_l$ distribution, and we use symmetric part from the $t\bar{t}$ samples at parton level, this methodology naturally corrects for the detector response and limited detector η coverage at the same time.

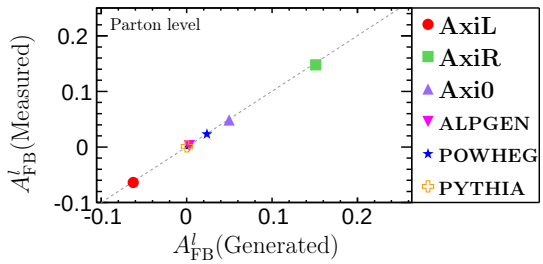

FIG. 3: A comparison between the predicted $A^l_{\rm FB}$ from simulations and the $A^l_{\rm FB}$ as measured using the $a \cdot \tanh$ parametrization with parton level information from $|q_l\eta_l| < 2.0$. The dashed line indicates the location of the equal values, while the points are superimposed at their measured locations. All the points lie along the line within uncertainties.

4.2. Parametrization Study

The functional form of $a \cdot \tanh$ is purely empirical. In this subsections, we show a detailed study of this methodology, and provide a semi-proof of this $a \cdot \tanh$ model.

A visual inspection of the distributions in Fig. 1 is suggestive of Gaussian descriptions of the $q_l\eta_l$ distributions, with the means shifted from zero. With detailed studies, we find that the sum of two Gaussian functions with the μ's forced to be the same works very well at describing the data, even at large values of $q_l\eta_l$. We have not uncovered a solid explanation why this should be so, but it appears to be true for all the models we considered. We use the functional form:

$$\frac{\mathrm{d}\mathcal{N}(q_l\eta_l)}{\mathrm{d}(q_l\eta_l)} = C\Big(e^{-\frac{(q_l\eta_l-\mu)^2}{2\sigma_1^2}} + re^{-\frac{(q_l\eta_l-\mu)^2}{2\sigma_2^2}}\Big), \qquad (7)$$

where C is a normalization constant, r is a multiplicative factor that covers the relative normalization of the two components and σ_1 and σ_2 are the widths of the two different distributions. Fig. 4 shows a comparison between the best fit and the parton level data. This functional form works well for all our benchmark signal samples. In addition, the two σ terms and the r term are found to be very consistent among all the benchmark signal samples, with the values of $\sigma_1 = 0.91$, $\sigma_2 = 1.61$ and $r = 0.11$. From here on, we assume the two σ terms and the r term have the best fit values from the benchmark samples for further studies.

We compare the parametrization with the $a \cdot \tanh$ model and the double-Gaussian model visually. Figure 5 shows the $\mathcal{A}(q_l\eta_l)$ term and the differential contribution to the inclusive $A^l_{\rm FB}$ as a function of $q_l\eta_l$ from the POWHEG sample, overlaid with the best fit from the $a\cdot\tanh$ model, the single-Gaussian model and the double-Gaussian model described in this article, when we only consider events with $|q_l\eta_l| < 2.0$. All three models fit

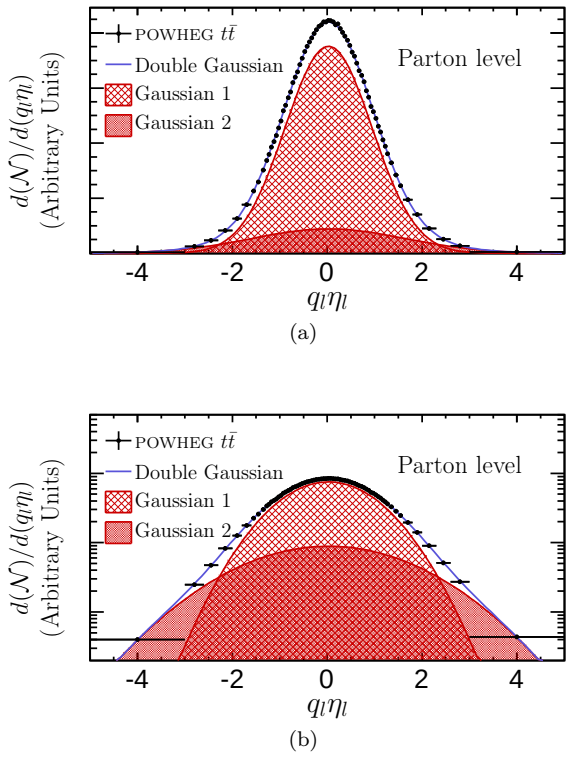

FIG. 4: The $q_l\eta_l$ distribution from the POWHEG $t\bar{t}$ sample at parton level, overlaid with the double-Gaussian fit. Note that both the tails and the central part of the distribution are well described.

this $q_l\eta_l$ region well. Since the region $|q_l\eta_l| < 2.0$ is where most of the contribution to $A^l_{\rm FB}$ comes from, all three models (including the single-Gaussian model) get back to the inclusive $A^l_{\rm FB}$ of the sample reasonably well. The double-Gaussian model fits the asymmetric part better in the $q_l\eta_l$ region above 2.0 than the tanh model, thus the differential contribution predicted by the double-Gaussian model lines up with the POWHEG predicted points marginally better. However, as stated earlier, the improvement is in the region where the contribution to the inclusive $A^l_{\rm FB}$ is small, thus the improvement in the resultant $A^l_{\rm FB}$ using the double-Gaussian model is very small. Fig. 6 shows the double-Gaussian model fit to the $\mathcal{A}(q_l\eta_l)$ distribution for all the six benchmark samples at parton level. A comparison with Fig. 2b shows that the double-Gaussian model matches all the simulated samples better than the $a\cdot\tanh$ model, although the differences are mostly in the high-$q_l\eta_l$ region where the contribution to the inclusive $A^l_{\rm FB}$ is small, and there is no data from the experiments in this region.

We next test how well the $a \cdot \tanh$ and the double-Gaussian methods reproduce the inclusive $A^l_{\rm FB}$ values for all 6 simulated samples with only events within $|q_l\eta_l| < 2.0$. A comparison of results is given in Table IV. Though the double-Gaussian model works better in the high $q_l\eta_l$

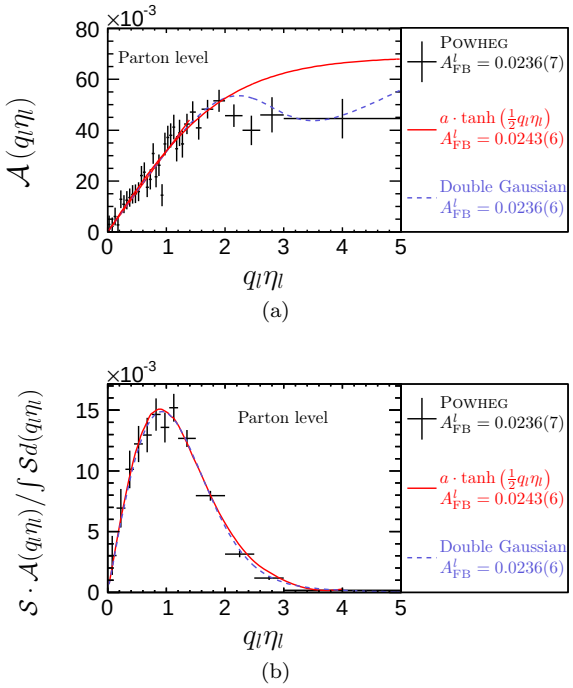

FIG. 5: Comparison between the $a \cdot \tanh$ model and the double-Gaussian model to the data from the POWHEG simulation. (a) shows the best fits of the $\mathcal{A}(q_l\eta_l)$ distribution (done only using events with $|q_l\eta_l| < 2.0$), while (b) shows the differential contribution to the $A^l_{\rm FB}$ as a function of $q_l\eta_l$ from different models.

region, the impact on the $A^l_{\rm FB}$ measurement is negligible compared to the dominant uncertainties in the measurement ($\sim$0.02 in the lepton+jets final state [12] and $\sim$0.05 in the dilepton final state [20]).

Model	True $A^l_{\rm FB}$	Measured $A^l_{\rm FB}$ ($a \cdot \tanh$ model)	Measured $A^l_{\rm FB}$ (Double-Gaussian model)
AxiL	-0.063(2)	-0.064(2)	-0.064(2)
AxiR	0.151(2)	0.148(2)	0.150(2)
Axi0	0.050(2)	0.048(2)	0.048(2)
ALPGEN	0.003(1)	-0.004(1)	0.002(1)
PYTHIA	0.001(1)	-0.005(1)	0.001(1)
POWHEG	0.023(1)	0.024(1)	0.023(1)

TABLE IV: Comparison of the predicted $A^l_{\rm FB}$ values and the corresponding measured $A^l_{\rm FB}$ values with the $a \cdot \tanh$ model and the double-Gaussian model. The uncertainties are statistical only and are always small compared to the expected statistics in data collected by CDF and D0 experiments.

In conclusion of this subsection, we now understand that this excellent approximation of the $\mathcal{A}(q_l\eta_l)$ term with the hyperbolic tangent function is fortuitous but robust, and the methodology of measuring the $A^l_{\rm FB}$ works at parton level. In the next subsection, we will test the methodology considering the effect of the detector simulation and the event reconstruction.

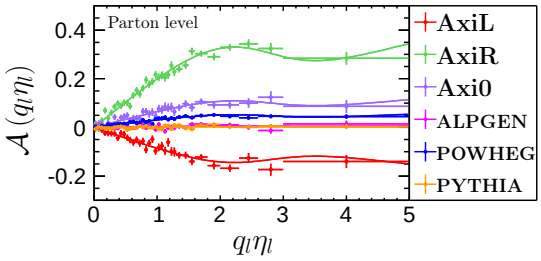

FIG. 6: Best fit of double-Gaussian model to the $\mathcal{A}(q_l\eta_l)$ distribution for various $t\bar{t}$ samples at parton level. This figure can be compared directly to Fig. 2b where we fit the same data, but using the $a \cdot \tanh$ function.

4.3. Methodology Validation at Reconstructed Level

Since we have limited statistics, imperfect detector resolution and incomplete detector coverage we next use simulated data from the different $t\bar{t}$ MC samples to see if there are any biases in our methodology or if further corrections are needed.

With the fit of Eqn. 6 on the $q_l\eta_l$ distribution after detector simulation and reconstruction in various $t\bar{t}$ MC samples, we obtain the measured values of $A^l_{\rm FB}$, and compare the results to the inclusive $A^l_{\rm FB}$ in corresponding MC sample at parton level. Figure 7 shows the reconstructed level $\mathcal{A}(q_l\eta_l)$ term from $t\bar{t}$ MC samples together with best fit of Eqn. 6. The results of the inclusive parton level $A^l_{\rm FB}$ are listed in Table V together with the corresponding inclusive $A^l_{\rm FB}$ at parton level. Figure 8 shows the comparison graphically. We note that with the method described above, we get back to the generated $A^l_{\rm FB}$ within statistics with no noticeable bias. The differences are small compared to expected statistical uncertainty around 0.05. To cover the potential bias caused by this method conservatively, we quote the difference between the measured parton level $A^l_{\rm FB}$ and the $A^l_{\rm FB}$ at parton level from POWHEG $t\bar{t}$ MC sample as the systematic uncertainty for asymmetric modelling.

CDF Run II Preliminary (9.1 fb^{-1})

Model	$A^l_{\rm FB}$(Generator Level)	$A^l_{\rm FB}$(Reco. Level)	Difference
AxiL	-0.063	-0.063±0.011	0.0001
AxiR	0.151	0.147±0.011	0.004
Axi0	0.050	0.065±0.011	-0.015
ALPGEN	0.003	-0.004±0.006	0.008
PYTHIA	0.000	-0.005±0.004	0.005
POWHEG	0.024	0.029±0.003	-0.006

TABLE V: Hyperbolic tangent fit on reconstructed level asymmetric part, and resultant $A^l_{\rm FB}$.

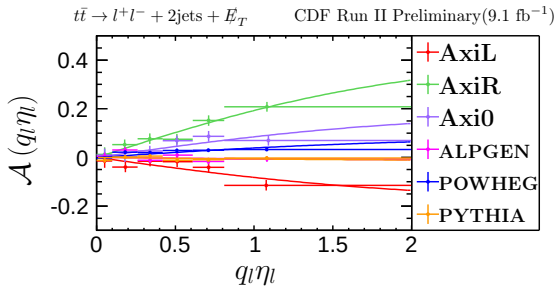

FIG. 7: Asymmetric part of $q_l\eta_l$ distribution for both positive and negative leptons from MC samples with various physics models at reconstructed level, with tanh fit.

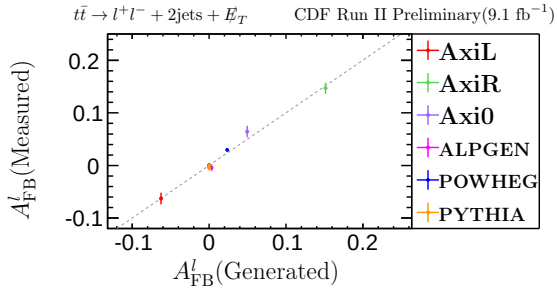

FIG. 8: Truth level $A_{\rm FB}^l$ vs. $A_{\rm FB}^l$ from tanh fit on the asymmetric part of $q_l\eta_l$ distribution at reconstructed level with symmetric part from POWHEG $t\bar{t}$ MC.

5. MEASURING $A_{\rm FB}$ FROM DATA

With the measurement methodology understood and validated, we can take the data at CDF in the dilepton final state, subtract off the backgrounds and extrapolate to get the measured $A_{\rm FB}^l$. In this section, we first show the $A_{\rm FB}$ obtained from data before and after subtracting off the background contamination without any correction, measure the parton level $A_{\rm FB}^l$ and give our estimate of the total uncertainties. A brief description of the measurement of the parton level $A_{\rm FB}^{ll}$ follows that.

5.1. Measuring $A_{\rm FB}^l$

With the signal region defined and background components estimated, we are ready to look at the distribution of $q_l\eta_l$ from data and compare to the SM expectation. The results are shown in Fig. 9. Fig. 10 shows the $\mathcal{S}(q_l\eta_l)$ term from data after background subtraction with expectation from POWHEG $t\bar{t}$ MC. Data after background subtraction shows good agreement with POWHEG $t\bar{t}$ MC. Figure 11 shows the best fit of Eqn. 6 on the $\mathcal{A}(q_l\eta_l)$ term of data after background subtraction. The $A_{\rm FB}^l$ retrieved from this fit is

$$A_{\rm FB}^l = 0.072 \pm 0.052(stat.)$$

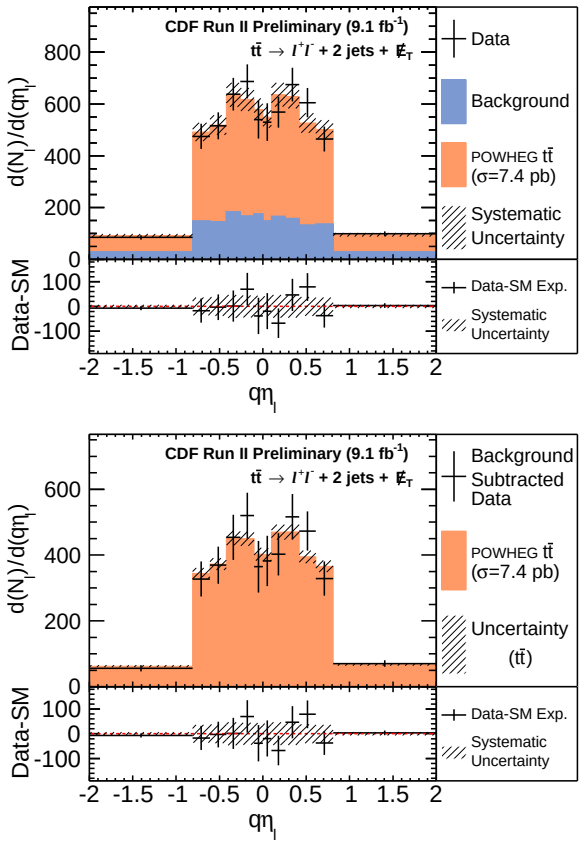

FIG. 9: $q_l\eta_l$ distribution of SM expectation overlaid with observation from data, as well as $q_l\eta_l$ distribution from POWHEG $t\bar{t}$ MC, overlaid with observation from data after subtracting off background contributions.

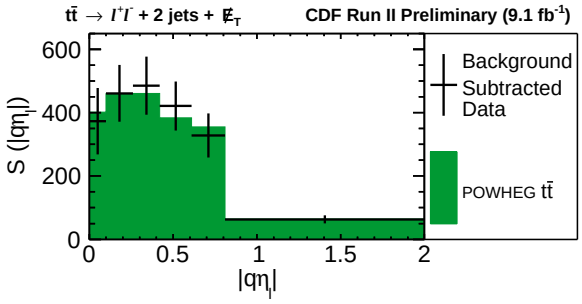

FIG. 10: Symmetric part of $q_l\eta_l$ distribution from data after background subtraction with expectation from POWHEG overlaid.

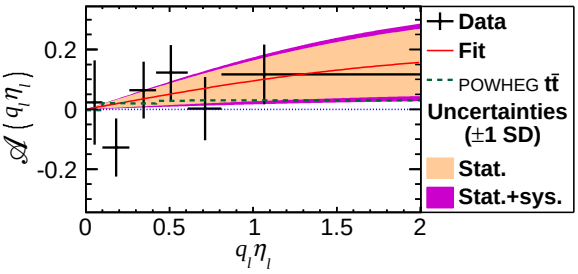

FIG. 11: Asymmetric part of $q_l\eta_l$ distribution from data after background subtraction. The green line shows expectation from POWHEG MC.

5.2. Systematic uncertainties for $A^l_{\rm FB}$

The systematic uncertainties are estimated using the similar techniques as for the measurement of $A^l_{\rm FB}$ in the lepton+jets final state [14]. As will be seen, the dominant uncertainty on the measurement is the statistical uncertainty, while the dominant systematic uncertainty is from the estimation of the background. The results are summarized in Table VI.

The dominant source of systematic uncertainty is due to the background uncertainties and is estimated to be ± 0.029 using pseudoexperiments, which covers both the uncertainties in the background normalizations and the uncertainties in modeling the $A^l_{\rm FB}$ of the backgrounds. The next most important source of systematic uncertainty is the ± 0.006 asymmetric-modeling contribution discussed above. The jet-energy-scale systematic uncertainty is estimated to be ± 0.004 by varying the jet energies within their uncertainties. The variations obtained by using the symmetric model from various MC samples are assigned as the symmetric-modeling systematic uncertainty, which is ± 0.001. Other sources of uncertainties due to the uncertainties in the parton showering model, the modeling of color reconnection, the amount of initial-state and final-state radiation, and the uncertainty on the parton distribution functions, are found to be negligible. The total systematic uncertainty, ± 0.03, is estimated by summing the individual contributions in quadrature.

After including all the systematic uncertainties, the parton level $A^l_{\rm FB}$ is measured as

$$A^l_{\rm FB} = 0.072 \pm 0.052(stat.) \pm 0.030(sys.) = 0.072 \pm 0.060$$

5.3. Measuring $A^{ll}_{\rm FB}$

The same method is also validated for measuring $A^{ll}_{\rm FB}$. With the same approach, we find the result as

$$A^{ll}_{\rm FB} = 0.076 \pm 0.072(\text{stat.}) \pm 0.039(\text{sys.}) = 0.072 \pm 0.082$$

.

CDF Run II Preliminary (9.1 fb^{-1})	
Source of Uncertainty ($A^l_{\rm FB}$)	Value
Backgrounds	0.029
Asymmetric Modeling	0.006
Jet Energy Scale	0.004
Symmetric Modeling	0.001
Total Systematic	0.030
Statistical	0.052
Total Uncertainty	0.060

TABLE VI: Table of uncertainties for $A^l_{\rm FB}$ measurement.

6. CDF COMBINATION OF $A^l_{\rm FB}$

In order to obtain a more sensitive measurement, we combine the dilepton measurement of $A^l_{\rm FB}$ with the CDF measurement in the lepton+jets final state reported in Ref. [12], $A^l_{\rm FB} = 0.094 \pm 0.024(\text{stat})^{+0.022}_{-0.017}(\text{syst})$. The combination is based on the asymmetric iterative algorithm of the *best linear unbiased estimates* approach [21, 22]. Since the measurements use statistically independent samples, the statistical uncertainties are uncorrelated. The background systematic uncertainties are treated as uncorrelated since they are mainly caused by the uncertainties in the modeling of the background $q_l\eta_l$ distributions, which are largely uncorrelated between the two measurements. The recoil-modeling systematic uncertainty in the lepton+jets measurement and the asymmetric-modeling systematic uncertainty in the dilepton measurement are both designed to cover the potential biases introduced by the measurement methodology, and are thus treated as fully correlated. The jet-energy-scale systematic uncertainties are also treated as fully correlated. The other systematic uncertainties are negligible in one of the two measurements, thus only the non-negligible part is included. The uncertainties are summarized in Table VII, as well as the correlations between the uncertainties in the two measurements.

The combined result is

$$A^l_{\rm FB} = 0.090^{+0.028}_{-0.026},$$

where 80% of the measurement weight is due to lepton+jets and 20% is due to dileptons. The difference in the weights is mostly due to the larger size of the lepton+jets final state sample. The correlation between the two measurement uncertainties is estimated to be 2.6%.

7. PROSPECT OF RECONSTRUCTION OF $t\bar{t}$ AND MEASUREMENT OF $A^{t\bar{t}}_{\rm FB}$

With the event selection and background modeling validated, and the measurement of $A^l_{\rm FB}$ and $A^{ll}_{\rm FB}$ completed, we now have the solid ground to measure the inclusive $A^{t\bar{t}}_{\rm FB}$ in the dilepton final state with full CDF II dataset.

CDF Run II Preliminary

Source of uncertainty	L+J (9.4fb^{-1})	DIL (9.1fb^{-1})	Correlation
Backgrounds	0.015	0.029	0
Recoil modeling (Asymmetric modeling)	$^{+0.013}_{-0.000}$	0.006	1
Symmetric modeling	-	0.001	
Color reconnection	0.0067	-	
Parton showering	0.0027	-	
PDF	0.0025	-	
JES	0.0022	0.004	1
IFSR	0.0018	-	
Total systematic	$^{+0.022}_{-0.017}$	0.030	
Statistics	0.024	0.052	0
Total uncertainty	$^{+0.032}_{-0.029}$	0.060	

TABLE VII: Table of uncertainties for $A^l_{\rm FB}$ measurement in the lepton+jets and the dilepton final state. In the column of correlation, "0" indicates no correlation and "1" indicates fully positive correlation.

There are two main procedures in this measurement, the full reconstruction of the 4-momentums of the top and the anti-top quarks and the unfolding procedure to correct the observed $A^{t\bar{t}}_{\rm FB}$ to the inclusive parton level $A^{t\bar{t}}_{\rm FB}$. The two procedures will be described in the following subsections.

7.1. $t\bar{t}$ Reconstruction

The reconstruction of the 4-momentums of the top and anti-top quarks is difficult in the dilepton final state. In this final state, there are two neutrinos missing, which indicates six unknown variables. The distinction between the b-quark jet and the anti-b-quark jet is also not available in CDF experiment, results in the ambiguity of the 4-momentums of the b and anti-b quarks. On the other hand, there are six constraints, two W boson masses, two top-quark masses, and two measured components in the $\not\!\!E_T$.

We will use a similar kinematic fitter algorithm that was used in measuring the $A^{t\bar{t}}_{\rm FB}$ in the dilepton final state with 5.1 fb^{-1} data [6]. The basic idea is illustrated with the formulas below:

$$\begin{aligned}
M^2_{l^+\nu} &= (E_{l^+}+E_\nu)^2-(\vec{p}_{l^+}+\vec{p}_\nu)^2 = M^2_W \\
M^2_{l^-\bar{\nu}} &= (E_{l^-}+E_{\bar{\nu}})^2-(\vec{p}_{l^-}+\vec{p}_{\bar{\nu}})^2 = M^2_W \\
M^2_{l^+\nu b} &= (E_{l^+}+E_\nu+E_b)^2-(\vec{p}_{l^+}+\vec{p}_\nu+\vec{p}_b)^2 = M^2_t \\
M^2_{l^-\bar{\nu}\bar{b}} &= (E_{l^-}+E_{\bar{\nu}}+E_{\bar{b}})^2-(\vec{p}_{l^-}+\vec{p}_{\bar{\nu}}+\vec{p}_{\bar{b}})^2 = M^2_t \\
(\vec{p}_\nu+\vec{p}_{\bar{\nu}})_x &= (\not\!\!E_T)_x \\
(\vec{p}_\nu+\vec{p}_{\bar{\nu}})_y &= (\not\!\!E_T)_y
\end{aligned} \tag{8}$$

With these constraints, there are still up to four possible solutions, as well as two choices due to the ambiguity of b-quark and anti-b-quark jets. In addition, since the $E_{\rm T}$ of the jets and the $\not\!\!E_T$ is measured with a relatively large resolution, two scale factors for jet $E_{\rm T}$ values and two scale factors for the two components of $\not\!\!E_T$ are introduced. Among the multiple solutions, the one with the least likelihood is chosen, with the likelihood term defined as

$$\begin{aligned}
\mathcal{L}(\vec{p}_\nu,\vec{p}_{\bar{\nu}},E_b,E_{\bar{b}}) =& P(p_z^{t\bar{t}})P(p_T^{t\bar{t}})P(M^{t\bar{t}})\times \\
& \frac{1}{\sigma_{\rm jet1}}\exp\left(-\frac{1}{2}\left(\frac{E^{\rm measure}_{\rm jet1}-E^{\rm fit}_{\rm jet1}}{\sigma_{\rm jet1}}\right)\right)\times\frac{1}{\sigma_{\rm jet2}}\exp\left(-\frac{1}{2}\left(\frac{E^{\rm measure}_{\rm jet2}-E^{\rm fit}_{\rm jet2}}{\sigma_{\rm jet2}}\right)\right)\times \\
& \frac{1}{\sigma^{\not\!\!E_T}_x}\exp\left(-\frac{1}{2}\left(\frac{\not\!\!E^{\rm measure}_x-\not\!\!E^{\rm fit}_x}{\sigma^{\not\!\!E_T}_x}\right)\right)\times\frac{1}{\sigma^{\not\!\!E_T}_y}\exp\left(-\frac{1}{2}\left(\frac{\not\!\!E^{\rm measure}_y-\not\!\!E^{\rm fit}_y}{\sigma^{\not\!\!E_T}_y}\right)\right),
\end{aligned} \tag{9}$$

where $P(p_z^{t\bar{t}})$, $P(p_T^{t\bar{t}})$ and $P(M^{t\bar{t}})$ are the probability density functions of the corresponding kinematic variables, and the σ parameters are the resolutions of the corresponding jet $E_{\rm T}$ or $\not\!\!E_T$ component, all derived from the POWHEG sample. As an outline of the performance of this procedure, Fig. 12 shows the difference between the rapidity of the (anti-)top quarks at the generator level and the rapidity of them from the output of the kinematic

fitter algorithm. For the majority of the top quarks, the algorithm is able to reconstruct the rapidity within 0.5 of the generator level rapidity, while the tails are constituted of the events where at least one jet is poorly measured, or the kinematic fitter algorithm picks a wrong solution.

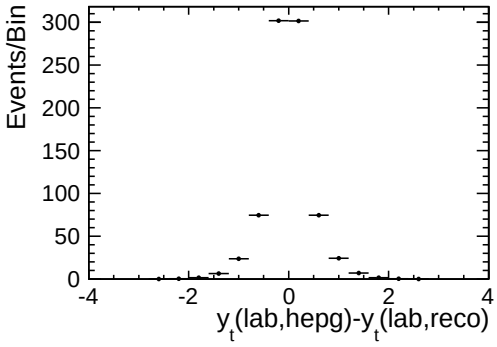

FIG. 12: The difference between the rapidity of the (anti-)top quarks at the generator level and the rapidity of them from the output of the kinematic fitter algorithm.

7.2. Unfolding of $A_{\rm FB}^{t\bar{t}}$

Due to the limited detector coverage, imperfect detector acceptance, the smearing caused by the detector and the possible biases introduced by the kinematic fitter algorithm an unfolding procedure is needed to measure the parton level inclusive $A_{\rm FB}^{t\bar{t}}$. Two steps are needed for this procedure. First, due to the smearing caused by the detector and the possible biases introduced by the kinematic fitter, the measured Δy_t is not necessarily the parton-level Δy_t. Figure 13 shows the detector response matrix for Δy_t, which captures these two effects. A regularized unfolding algorithm based on *single value decomposition* (SVD) will be used to calculate the inversion of the response matrix under certain regularization condition. The second step is to correct for the detector acceptance and the limited detector coverage. To correct for these effects, a bin-by-bin acceptance correction factor will be applied to obtain the inclusive parton-level $A_{\rm FB}^{t\bar{t}}$.

Once the $A_{\rm FB}^{t\bar{t}}$ measurement in the dilepton final state is produced, we will proceed to combine this measurement with the previous measurement in the lepton+jets final state to obtain the measurement of $A_{\rm FB}^{t\bar{t}}$ at CDF.

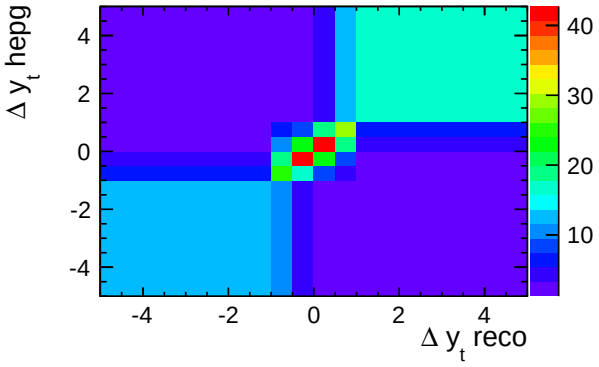

FIG. 13: The detector response matrix for Δy_t.

8. PROSPECT OF PRODUCING TEVATRON COMBINATION OF $A_{\rm FB}^{l}$, $A_{\rm FB}^{ll}$ AND $A_{\rm FB}^{t\bar{t}}$.

With the measurement of $A_{\rm FB}^{l}$, $A_{\rm FB}^{ll}$ completed, the measurement of $A_{\rm FB}^{t\bar{t}}$ in progress, and the corresponding measurements at D0 also produced, we are hoping to combine the measurements at both experiments and produce the Tevatron combination of these observables. These will be the Tevatron legacy results, producing the most sensitive measurements of these important observables at Tevatron.

9. CONCLUSION

The $A_{\rm FB}$ of the top-quark pairs from the $p\bar{p}$ collisions and $A_{\rm FB}$ of the charged leptons produced by the cascade decay of $t\bar{t}$ pairs produce a unique possibility to test the SM and probe the physics beyond the SM. We are working with the full dataset collected during CDF run II in the dilepton final state to produce a full analysis of the $A_{\rm FB}^{t\bar{t}}$, the $A_{\rm FB}^{l}$ and the $A_{\rm FB}^{ll}$, as well as the combinations of these observables at CDF and at the Tevatron.

We have finished measuring the $A_{\rm FB}^{l}$ and $A_{\rm FB}^{ll}$ in the dilepton final state using data collected during CDF Run II. The results are:

$$A_{\rm FB}^{l} = 0.072 \pm 0.052(\text{stat.}) \pm 0.030(\text{sys.}) = 0.072 \pm 0.060$$

and

$$A_{\rm FB}^{ll} = 0.076 \pm 0.072(\text{stat.}) \pm 0.039(\text{sys.}) = 0.076 \pm 0.082$$

The results are in consistent with the prediction from NLO SM of $A_{\rm FB}^{l} = 0.038 \pm 0.003$ and $A_{\rm FB}^{ll} = 0.048 \pm 0.004$ [4]. Furthermore we obtained the best measurement of the $A_{\rm FB}^{l}$ from CDF by combining the measurement in the lepton+jets final state with the measurement in the dilepton final state. The combined result is

$$A_{\rm FB}^{l} = 0.090^{+0.028}_{-0.026}$$

This result is 2σ larger than the NLO SM calculation.

We are finalizing the publication of the results of A^{l}_{FB} and A^{ll}_{FB} in the dilepton final state at CDF, as well as the A^{l}_{FB} combination at CDF. In the mean time, we are working on the kinematic fitter algorithm and the unfolding process to measure the inclusive parton-level $A^{t\bar{t}}_{\mathrm{FB}}$ in the dilepton final state at CDF, as well as the combination of $A^{t\bar{t}}_{\mathrm{FB}}$ at CDF. We are also looking forward to work on the Tevatron combination of A^{l}_{FB}, A^{ll}_{FB} and $A^{t\bar{t}}_{\mathrm{FB}}$ if possible.

[1] T. Aaltonen *et al.* (CDF Collaboration), Phys. Rev. D **87**, 092002 (2013).

[2] V. Abazov *et al.* (D0 Collaboration), Phys. Rev. D **84**, 112005 (2011).

[3] T. Aaltonen *et al.* (CDF Collaboration), Phys. Rev. Lett. **111**, 182002 (2013).

[4] W. Bernreuther and Z.-G. Si, Phys. Rev. D **86**, 034026 (2012).

[5] W. Bernreuther and Z.-G. Si, Nucl. Phys. **B837**, 90 (2010).

[6] T. Aaltonen *et al.* (CDF Collaboration), CDF Public Note 10436 (2011).

[7] D.-W. Jung, P. Ko, and J. S. Lee, Phys. Lett. B **701**, 248 (2011); D.-W. Jung, P. Ko, J. S. Lee, and S. hyeon Nam, *ibid.* **691**, 238 (2010); P. H. Frampton, J. Shu, and K. Wang, *ibid.* **683**, 294 (2010); E. Álvarez, L. Rold, and A. Szynkman, J. High Energy Phys. 05 (2011) 070; C.-H. Chen, G. Cvetic, and C. Kim, Phys. Lett. B **694**, 393 (2011); Y.-k. Wang, B. Xiao, and S.-h. Zhu, Phys. Rev. D **82**, 094011 (2010); A. Djouadi, G. Moreau, F. m. c. Richard, and R. K. Singh, *ibid.* **82**, 071702 (2010); R. S. Chivukula, E. H. Simmons, and C.-P. Yuan, *ibid.* **82**, 094009 (2010); B. Xiao, Y.-k. Wang, and S.-h. Zhu, *ibid.* **82**, 034026 (2010); Q.-H. Cao, D. McKeen, J. L. Rosner, G. Shaughnessy, and C. E. M. Wagner, *ibid.* **81**, 114004 (2010); I. Doršner, S. Fajfer, J. F. Kamenik, and N. Košnik, *ibid.* **81**, 055009 (2010); S. Jung, H. Murayama, A. Pierce, and J. D. Wells, *ibid.* **81**, 015004 (2010); J. Shu, T. M. P. Tait, and K. Wang, *ibid.* **81**, 034012 (2010); A. Arhrib, R. Benbrik, and C.-H. Chen, *ibid.* **82**, 034034 (2010); J. Cao, Z. Heng, L. Wu, and J. M. Yang, *ibid.* **81**, 014016 (2010); V. Barger, W.-Y. Keung, and C.-T. Yu, *ibid.* **81**, 113009 (2010); P. Ferrario and G. Rodrigo, *ibid.* **78**, 094018 (2008); **80**, 051701 (2009); M. Bauer, F. Goertz, U. Haisch, T. Pfoh, and S. Westhoff, J. High Energy Phys. 11 (2010) 039; K. Cheung, W.-Y. Keung, and T.-C. Yuan, Phys. Lett. B **682**, 287 (2009).

[8] A. Falkowski, M. L. Mangano, A. Martin, G. Perez, and J. Winter, Phys. Rev. D **87**, 034039 (2013).

[9] J. Kühn and G. Rodrigo, J. High Energy Phys. 01 (2012) 063; A. V. Manohar and M. Trott, Phys. Lett. B **711**, 313 (2012); W. Hollik and D. Pagani, Phys. Rev. D **84**, 093003 (2011).

[10] T. Sjostrand, S. Mrenna, and P. Z. Skands, J. High Energy Phys. 05 (2006) 026.

[11] M. L. Mangano, M. Moretti, F. Piccinini, R. Pittau, and A. D. Polosa, J. High Energy Phys. 07 (2003) 001.

[12] T. Aaltonen *et al.* (CDF Collaboration), Phys. Rev. D **88**, 072003 (2013).

[13] V. Abazov *et al.* (D0 Collaboration), D0 Note 6394-CONF (2013).

[14] V. M. Abazov *et al.* (D0 Collaboration), Phys. Rev. D **88**, 112002 (2013).

[15] D. Acosta *et al.* (CDF Collaboration), Phys. Rev. D **71**, 032001 (2005).

[16] T. Aaltonen *et al.* (CDF Collaboration), Phys. Rev. D **88**, 091103 (2013).

[17] U. Baur, T. Han, and J. Ohnemus, Phys. Rev. D **48**, 5140 (1993).

[18] E. Gerchtein and M. Paulini, eConf **C0303241**, TUMT005 (2003), arXiv:physics/0306031.

[19] S. Agostinelli *et al.*, Nucl. Instrum. Methods A **506**, 250 (2003).

[20] T. Aaltonen *et al.* (CDF Collaboration), CDF Public Note 11035 (2013).

[21] L. Lyons, D. Gibaut, and P. Clifford, Nucl. Instrum. Methods A **270**, 110 (1988); L. Lyons, A. J. Martin, and D. H. Saxon, Phys. Rev. D **41**, 982 (1990); A. Valassi, Nucl. Instrum. Methods A **500**, 391 (2003).

[22] R. Group, C. Ciobanu, K. Lannon, and C. Plager, in *Proceedings of the 34th International Conference in High Energy Physics (ICHEP08), Philadelphia, 2008, eConf C080730*, arXiv:0809.4670.